Spectroscopy of Hydrogenic Atoms

Dennis V. Perepelitsa* and Brian J. Pepper†
MIT Department of Physics
(Dated: October 23, 2006)

The emission spectra of several hydrogenic species are investigated, after calibration from the principal lines of mercury, using a high-resolution monochromator. The Balmer lines of hydrogen are measured, as are many visible transitions of sodium, each to a relatively high degree of precision. The Rydberg constant is calculated at $R_H = 10970730 \pm 30\ \mathrm{m}^{-1}$. The hydrogen isotope shift is measured, and a value for the deuteron to proton mass ratio is calculated at $\frac{m_D}{m_H} = 1.99 \pm .09$.

1. INTRODUCTION

The emission spectra of hydrogenic atoms have been investigated since the early 20th century for their relative simplicity and importance. The quantized nature of the mathematical models that seemed to predict the behavior of hydrogen emissions were one of the early indications of quantum theory.

Even multiply-ionized atoms with a single electron, and atoms with only a single electron outside of a series of "closed" shells are hydrogenic in this respect. Furthermore, small distortions in the emission spectra give insight into the structure of the atom. For example, smaller, observed spectral lines close to the ones of hydrogen caused physicists to predict the existence of deuterium.

In this paper, we investigate quantitatively the fitness of the Rydberg equation, calculate the Rydberg constant, and investigate two such corrections: the hydrogen isotope shift, and the fine structure of sodium.

2. THEORY

It is well-known that an electron in an energy level higher than the ground state can de-excite and fall to a lower energy level, emitting a photon. In general, an electron transitioning from the n_1 to the n_2 energy level bound to an atom with nuclear charge Ze has energy given by the non-relativistic Bohr equation:

$$\frac{1}{hc}E_{n_1 \to n_2} = \frac{1}{\lambda} = R_H Z^2 \left(\frac{1}{n_2^2} - \frac{1}{n_1^2}\right) \tag{1}$$

Where $R_H = \frac{1}{2} m_e c^2 \alpha^2$ is the Rydberg constant, Z is the atomic number, m_e is the mass of the electron, c is the speed of light, and α is the fine-structure-constant discussed in Gasiorowicz [1]. We intend to measure the value of R_H using the Balmer lines (transitions that end in $n_2 = 2$) of hydrogen ($Z = 1$); these fall in the visible part of the spectrum.

*Electronic address: dvp@mit.edu
†Electronic address: bpepper@mit.edu

2.1. Isotope shift of hydrogen

During the derivation of (1), the nucleus was assumed to be a be a fixed center of force. In reality, the electron also attracts the nucleus, leading to energy levels that deviate slightly from the predicted values. According to French and Taylor [2], we can correct for this. In an atom with nuclear mass m_A, we replace the mass of the electron with a reduced mass

$$\mu = \frac{m_e m_A}{m_A + m_e} \tag{2}$$

There is therefore an expected *isotope shift* $\Delta\lambda = \lambda_H - \lambda_D$ between the spectral lines of hydrogen and deuterium. The difference in transition energies in the two isotopes is given by

$$\frac{1}{\lambda_H} - \frac{1}{\lambda_H - \Delta\lambda} = (\mu_H - \mu_D)\frac{R_H}{m_e}\left(\frac{1}{n_2^2} - \frac{1}{n_1^2}\right) \tag{3}$$

2.2. Fine structure

In reality, it is observed that more than a single spectral line corresponds a given energy level transition. This is because an electron in a given energy level also has an angular momentum, classified by orbital S, P, D or F, which imparts a slightly different binding energy. For example, the $3S$ level of sodium lies at a lower energy than the $3P$ energy level because there is less effective shielding of the electron from nuclear charge in the $3S$ orbital than in the $3P$. Thus we see distinct lines that correspond to this difference in the second quantum number.

Because of space constraints, we only classify various sodium lines here.

3. EXPERIMENTAL SETUP

The experimental setup consisted of high-resolution Jobin Yvon 1250M monochromator connected through a Mini-Step Driver Unit and an Acquisition Unit to a computer running LabView software. Two gratings were present in the monochromator, one with 1800

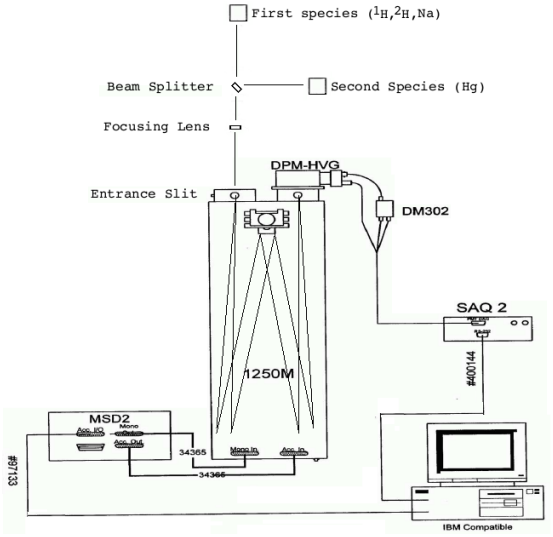

FIG. 1: Schematic of our experimental setup. Modified from the Lab Guide [3].

grooves/mm, and one with 3600 grooves/mm. Incident radiation fell across the entrance slit and collected at a spherical mirror in the back of the machine. A rotating grating selected out desired frequencies, and sent them through another spherical mirror, through an exit slit to a photomultiplier tube which measured the intensity of that frequency.

The maximal resolution on the two gratings was .04Å and .02Å, respectively. Furthermore, because of equipment limitations, we were unable to scan higher than 5000Å using the 3600 gvs./mm. grating. Using this grating therefore gave us more precise data, but could not be used to scan some of the spectra of interest.

Random sources of error in the monochromator include the uncertainty inherent in our step-size (.04Å for 1800 gvs./mm. and .02Å for 3600 gvs./mm.), and the repeatability error, given by the Installation Report [4] as $\sigma_r = .02$Å for 1800 gvs./mm., and $\sigma_r = .01$Å for 3600 gvs./mm. We intend to incorporate the former by fitting our spectra to a curve; this is discussed below.

Systematic sources of error include a small wavelength offset of what is indicated by the instrument from reality, which we take into account.

3.1. Procedure

To defeat the systematic error, we began each session with a calibration off the mercury spectrum. Often, we would use a beam splitter to superimpose the mercury spectrum over the spectrum of interest. Before each scan, we ensured that the apparatus had been reset, the photomultiplier voltage was turned on and that the lines were focused and fell directly across the entrance slit.

We then conducted broad scans, typically at $\Delta\lambda = 1$Å intervals, and detailed scans around areas of interest. We often used the CRC [5] and Melissinos [6] to confirm that we were looking at principal lines of hydrogen and sodium, respectively.

4. DATA AND ANALYSIS

4.1. Spectral line fitting

The observed spectral lines appear distributed about some mean with a significant width. We expect a number of phenomena to be contributing to this effect. Among them, the thermal Doppler shift, natural line widening due to uncertainty in the lifetime of the emitted particles, and collisions in the wavetrain, contribute to frequency spread.

To model this, we used the Voigt profile, a convolution of Gaussian and Lorentzian profiles, commonly used in optical spectroscopy. The degree to which it is "Gaussian" and "Lorentzian" are given by the parameters σ and γ, respectively. The probability distribution for a Voigt profile centered at λ_0 is given by:

$$P(\lambda;\lambda_0,\sigma,\gamma) = \frac{\mathrm{Re}[w(\frac{(\lambda-\lambda_0)+i\gamma}{\sigma\sqrt{2\pi}})]}{\sigma\sqrt{2\pi}} \tag{4}$$

Where $Re[w(z)]$ is the real part of the complex error function. We fitted every spectral line to a Voigt profile using MATLAB's `fitnonlin.n` routine, and recorded the center point λ_0 (and its uncertainty, respectively) as the wavelength λ corresponding to that line (as the error σ_V, respectively[1]). σ_V ranged from .03Å for some of the tighter fits to .10Å on some of the noisier lines.

4.2. Mercury calibration

A salient feature of our data is that the wavelengths appear to be consistently shifted 1-3Å higher from their expected value. We treated this as a systematic error in the monochromator gratings, and made sure to calibrate each data set by accepted values of the prominent spectral lines of mercury: roughly, the ones at 3650Å, 4047Å, 4358Å, 5460Åand 5770Å.

Specifically, for a set of systematic offsets from the mercury lines, we took the weighted mean as the calibration offset $\Delta\lambda_c$, with the uncertainty in each measurement as the metric. We similarly calculated the error in the calibration offset, using Bevington [7]:

$$\Delta\lambda_c = \sum_n (\Delta\lambda_n/\sigma_n)^2 / \sum_n (1/\sigma_n)^2 \tag{5}$$

$$\sigma_c^2 = 1/\sum_n (1/\sigma_n)^2 \tag{6}$$

[1] Not to be confused with the parameter σ in the Voigt profile equation above.

Under the 1800 gvs./mm. grating, the systematic calibration offset $\Delta\lambda_c$ ranged from $-.95$ Å to -1.23 Å , and from -2.89Å to -3.09Å under the 3600 gvs./mm. The error in the calibration offset was on the order of $\sigma_c = .01 - .03$ Å.

This tactic of taking the weighted mean of a number of calculated values is one we will use later.

4.3. Sources of error

We have encountered several sources of error in the determination of the wavelength of a given spectral line. To determine the uncertainty in the calculation of the wavelength of any spectral line, we must consider three sources of error: the uncertainty in the calculation of the calibration offset σ_c, the uncertainty in fitting the wavelength to a Voigt profile σ_V, and the repeatability error σ_r at that resolution measured in the Installation Report [4]. These are all uncorrelated errors that will skew the calculation of the line linearly. Thus, the error associated with the calculation of any wavelength λ is

$$\sigma_\lambda^2 = \sigma_{\mathrm{C}}^2 + \sigma_{\mathrm{V}}^2 + \sigma_{\mathrm{r}}^2 \tag{7}$$

4.4. Determination of the Rydberg constant

Under 1800 gvs./mm. and 3600 gvs./mm., we were able to distinguish the first seven and six hydrogen Balmer lines, respectively. The values are given in Table I. The Rydberg constant varies inversely with λ, and has relative error proportional to that of λ:

$$R_H = \frac{1}{\lambda_H}\left(\frac{1}{4} - \frac{1}{n^2}\right)^{-1}, \quad \frac{\sigma_{R_H}}{R_H} = -\frac{\sigma_\lambda}{\lambda} \tag{8}$$

We calculate the weighted average and weighted error of these thirteen data points using the same methodology in (6), and arrive at a value $R_H = 10970730 \pm 30$ m^{-1}.

TABLE I: Calculated Balmer lines of hydrogen

Accepted		**1800 gvs./mm.**	**3600 gvs./mm.**
Line	λ	λ_{1800}	λ_{3600}
$3 \to 2$	6562.85Å	6562.95 ± .07Å	-
$4 \to 2$	4861.36Å	4861.40 ± .08Å	4861.66 ± .03Å
$5 \to 2$	4340.46Å	4340.43[b] ± .07Å	4340.52 ± .03Å
$6 \to 2$	4101.74Å	4101.77 ± .08Å	4101.74 ± .03Å
$7 \to 2$	3970.07Å	3970.07 ± .08Å	3970.16 ± .03Å
$8 \to 2$	3889.05Å	3889.11 ± .08Å	3889.04 ± .03Å
$9 \to 2$	3835.39Å	3835.40 ± .09Å	3835.44 ± .03Å

[b]This data point was taken from the Deuterium data set; the actual point was lost due to experimenter confusion.

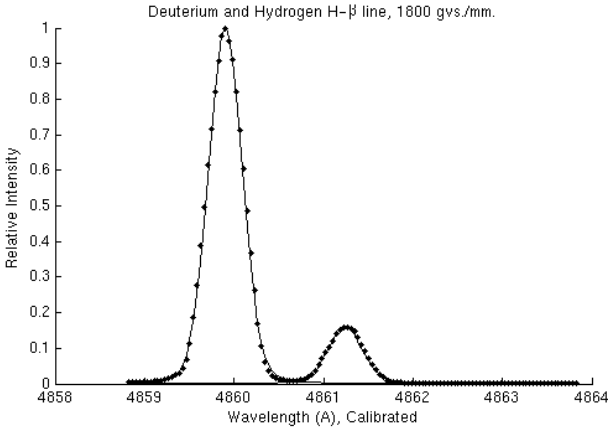

FIG. 2: The H_β and D_β lines at 1800 gvs./mm., fitted with Voigt profiles.

4.5. Determination of the hydrogen isotope mass ratio

Figure 2 shows a typical close-up scan of a deuterium spectral line. The smaller line on the right leads us to believe that the deuterium lamp is contaminated with ordinary hydrogen. We fitted both peaks with Voigt profiles, observing that the isotope shift increases as the wavelength does. We can algebraically manipulate (3) into a form that isolates the mass ratio:

$$\frac{m_D}{m_H} = \frac{m_e}{m_H}\left(\frac{1 + \frac{m_e}{m_H}}{1 - \frac{\Delta\lambda}{\lambda_H}} - 1\right)^{-1} \tag{9}$$

Using the established value $\frac{m_e}{m_H} = \frac{1}{1836.15}$, we obtain several values for $\frac{m_D}{m_H}$ versus $\frac{\Delta\lambda}{\lambda}$. These are shown in Table II.

TABLE II: Calculated deuteron-to-proton mass ratios.

1800 gvs./mm.			**3600 gvs./mm.**		
λ_H	$\Delta\lambda$	m_D/m_H	λ_H	$\Delta\lambda$	m_D/m_H
6562.95Å	-1.77Å	1.98 ± .16		-	
4861.40Å	-1.34Å	2.03 ± .16	4861.66Å	-1.32Å	1.99 ± .08
4340.43Å	-1.19Å	2.01 ± .18	4340.52Å	-1.14Å	1.93 ± .10
4101.77Å	-1.10Å	1.97 ± .22	4101.74Å	-1.13Å	2.02 ± .12
3970.07Å	-1.06Å	1.96 ± .30	3970.16Å	-1.11Å[b]	2.06 ± .18

[b]The smaller hydrogen line was indistinguishable, so we use a previously determined value.

We determine the error on this calculation. Conservatively, the error in fitting the hydrogen and deuterium lines, but not the calibration and repeatability errors, which would cancel in the difference, contribute to the error inherent in the calculation of $\Delta\lambda$. Further algebraic manipulation of (9) leads to simple relation between

TABLE III: Classification of sodium doublets.

Theoretical		1800 gvs./mm.	3600 gvs./mm.
7D → $3P_{1/2}$	4494.18Å	4494.31 ± .04Å	4494.17 ± .07Å
7D → $3P_{3/2}$	4497.66Å	4497.70 ± .03Å	4497.69 ± .04Å
6D → $3P_{1/2}$	4664.81Å	4664.92 ± .11Å	4664.85 ± .03Å
6D → $3P_{3/2}$	4668.56Å	4668.69 ± .09Å	4668.64 ± .03Å
7S → $3P_{1/2}$	4747.94Å	4748.12 ± .16Å	4748.09 ± .07Å
7S → $3P_{3/2}$	4751.82Å	4752.00 ± .13Å	4751.86 ± .04Å
5D → $3P_{1/2}$	4978.54Å	4978.55 ± .07Å	4979.26 ± .03Å
5D → $3P_{3/2}$	4982.81Å	4982.82 ± .07Å	4983.32 ± .02Å
6S → $3P_{1/2}$	5148.84Å	5148.99 ± .08Å	-
6S → $3P_{3/2}$	5153.40Å	5153.54 ± .07Å	-
4D → $3P_{1/2}$	5682.63Å	5682.83 ± .06Å	-
4D → $3P_{3/2}$	5688.21Å	5688.39 ± .06Å	-
$3P_{3/2}$ → 3S	5889.95Å	5890.10 ± .07Å	-
$3P_{1/2}$ → 3S	5895.92Å	5896.03 ± .07Å	-
5S → $3P_{1/2}$	6154.23Å	6154.40 ± .06Å	-
5S → $3P_{3/2}$	6160.75Å	6160.89 ± .06Å	-

σ_{m_D/m_H} and $\sigma_{\Delta\lambda}$.

$$\sigma^2_{\Delta\lambda} \sim \sigma^2_{V-\lambda_H} + \sigma^2_{V-\lambda_D} \tag{10}$$

$$\frac{\sigma_{m_D/m_H}}{m_D/m_H} = \frac{\sigma_{\Delta\lambda}}{\Delta\lambda} \tag{11}$$

With this formulation of the error, we calculate the weighted mean and weighted error, as we did in (6), of the nine data points, yielding a value of $\frac{m_D}{m_H} = 1.99 \pm .09$.

4.6. Classification of the sodium doublets

The fine structure splitting of sodium lines was very visible. We have identified these lines with the aid of Melissinos [6] and calculated their wavelength. The results are shown in Table III.

5. CONCLUSIONS

In general, our findings are in good agreement with accepted values.

The calculation of the Balmer lines at 1800 gvs./mm., in particular, is correct to an error on the order of hundredths of an Angstrom, as are many of our best calculations of principal sodium lines.

Our value of the mass ratio of the deuteron to the proton $\frac{m_D}{m_H} = 1.99 \pm .09$ is in excellent agreement with the expected value of $\frac{m_D}{m_H} = 2.00$, as is our calculated value of the Rydberg constant $R_H = 10970730 \pm 30\ \mathrm{m}^{-1}$, which has a .01% error from the accepted value of $10973730 m^{-1}$, despite the small error bars.

We have no obvious explanation for why our error bars are significantly lower than the deviation from the accepted value. It may simply not be possible to calculate R_H to better than this .01% without using a Bohr equation corrected for mass, relativistic and spin effects.

Finally, there were complications from fitting the spectral lines to Voigt profiles. Though in general, good fits were calculated by the computer, the resultant γ and σ parameters varied wildly and often had uncertainties larger than their values. We found that we could not account for the shape of the spectral lines using thermal Doppler widening and natural line widening alone. In particular, we failed to properly investigate the calibration of the entrance and exit slits of the apparatus.

An improperly tuned exit slit could have smeared our spectral lines past the point of theoretical effects. Regrettably, this undoubtedly had adverse effects on the precision and accuracy of our data.

Length limitations have kept us from giving an in-depth treatment of the doublet separation of our sodium spectral lines. The comparison of our results with those predicted by fine structure theory is a rich possibility for further exploration.

[1] S. Gasiorowicz, *Quantum Physics* (Wiley, 2003), 3rd ed.

[2] A.P.French and E.F.Taylor, *An Introduction to Quantum Physics* (Norton, 1978).

[3] J. L. Staff, *Optical spectroscopy of hydrogenic atoms* (2005), jLab E-Library, URL `http://web.mit.edu/8.13/www/JLExperiments/JLExp17.pdf`.

[4] *Spex 1250m installation report*, Available on: `https://web.mit.edu/8.13/8.13d/manuals/Hydrogenic/jy-1250m-installation-report-june-2002.pdf` (2002), jLab E-Library.

[5] R. C. Weast, ed., *CRC Handbook of Chemistry and Physics* (CRC Press, 1989), 69th ed.

[6] A. Melissinos, *Experiments in Modern Physics* (Academic Press, 1966).

[7] P. Bevington and D. Robinson, *Data Reduction and Error Analysis for the Physical Sciences* (McGraw-Hill, 2003).

Acknowledgments

DVP gratefully acknowledges Brian Pepper's equal partnership in the preparation and execution of the experiment, and the advice and guidance of Professor Isaac Chuang, Dr. Scott Sewell and Scott Sanders throughout the course of the experiment.